Catalysis Science & Technology

Accepted Manuscript

ROYAL SOCIETY OF CHEMISTRY

www.rsc.org/catalysis

Submitted to Catalysis Science & Technology

Type of paper: Original Research paper

Catalytic Behaviors of Ni/γ-Al_2O_3 and Co/γ-Al_2O_3 during the Hydrodeoxygenation of Palm Oil

Atthapon Srifa [a,b], Nawin Viriya-empikul [a], Suttichai Assabumrungrat [b], Kajornsak Faungnawakij [a,*]

[a] Nanomaterials for Energy and Catalysis Laboratory, National Nanotechnology Center (NANOTEC), National Science and Technology Development Agency (NSTDA), 111 Thailand Science Park, Thanon Phahonyothin, Tambon Khlong Nueng, Amphoe Khlong Luang, Pathum Thani 12120, Thailand

[b] Center of Excellence in Catalysis and Catalytic Reaction Engineering, Department of Chemical Engineering, Faculty of Engineering, Chulalongkorn University, Bangkok 10330, Thailand

* To whom correspondence should be addressed.

Tel.: +66–2–564–7100 ext. 6638; Fax: +66–2–564–6981

Email address: kajornsak@nanotec.or.th (K. Faungnawakij)

Abstract

The deactivation and regeneration behaviors of the Ni/γ-Al_2O_3 and Co/γ-Al_2O_3 catalysts in the hydrodeoxygenation (HDO) of palm oil were investigated at 573 K and 5 MPa in a trickle bed reactor. The catalysts were prereduced at 773 K for 3 h before the HDO experiments. The catalysts exhibited good catalytic activity (>90% yield) and remained stable for 100 h on-stream. Nevertheless, after 150 h on-stream, the product yield gradually decreased from 92.2 to 76.2% over the Ni catalyst and dramatically declined from 88.6% to ca. 56.6% over the Co catalyst. The combined decarbonylation and/or decarboxylation (DCO_x) reactions were dominant over the HDO reaction when the reaction was catalyzed by the Ni catalyst. Meanwhile, the contribution of DCO_x and HDO reactions were nearly comparable over the Co catalyst. The XRD and XANES analyses confirmed the partial formation of metallic nickel or cobalt after prereduction, and the further *in situ* reduction during the HDO experiments, suggesting the coexistence of the metal and metal oxides on the catalyst surfaces. The XRD and TEM analyses revealed some sintering of the nickel and cobalt particles during the time course of reaction. Based on the TPO analysis, the carbon deposition rate on cobalt catalyst was faster than that on nickel catalyst and would be a major reason for the catalyst deactivation, and the sintering was a minor one. Additionally, the regeneration under air at 773 K followed by reduction in H_2 at 773 K can completely restore the catalytic activity.

Keyword: Deactivation, Regeneration, Hydrodeoxygenation, Green diesel, Palm oil

1. Introduction

The development of liquid transport fuels from renewable bioresources is an important key to future energy sources due to the depletion of petroleum fuels. Biomass

feedstocks can be divided into three categories: carbohydrates (i.e., starch and sugar), lignocellulose materials, and animal fats/vegetable oils composed of triglycerides and free fatty acids ranging from C_{10}-C_{20} [1]. Triglycerides have been used as important renewable feedstocks for the production of liquid biofuels because of their low degree of functionalization and simple structure compared with cellulosic biomass [2, 3]. In particular, palm oil contains primarily C_{16} and C_{18} fatty acids, making it a promising feedstock for green diesel and biodiesel production. The conventional technology for conversion of animal fats/vegetable oils into the diesel-like fuels is a transesterification of triglycerides and methanol that produces the fatty acid methyl esters (FAMEs), which is called biodiesel [1, 4]. However, some disadvantages of biodiesel compared with petroleum diesel are the C=C bonds and C=O bonds that remain in the molecules of FAMEs, which leads to low thermal and oxidation stability because of its high oxygen content, high viscosity, and low heating value [5, 6].

Another effective way to use triglycerides for the production of diesel fuel is through hydrodeoxygenation, which removes oxygen functionalities from the triglycerides/free fatty acids at 573–623 K with H_2 at 5–15 MPa in the presence of heterogeneous catalysts [7, 8]. Green diesel, which provides better diesel properties, such as high cetane number, zero oxygen content [9], and high thermal and oxidation stability [10], can be produced by the catalytic deoxygenation of triglycerides through 3 major reaction pathways, including decarbonylation, decarboxylation, and hydrodeoxygenation [3, 11, 12], thus producing straight-chain alkanes ranging from C_{15} to C_{18}. First, the reaction proceeds via hydrogenation of unsaturated triglycerides (C=C double bond) to form saturated triglycerides [13], followed by hydrogenolysis of saturated triglycerides resulting in fatty acids and propane. Finally, the fatty acid undergoes the following reactions: (1) hydrodeoxygenation (HDO), an exothermic reaction, which removes oxygen in the form of water and yields n-alkanes with the same

carbon number as the corresponding fatty acid, (2) decarbonylation (DCO) and (3) decarboxylation (DCO_2), endothermic reactions, which lead to elimination of oxygen in the form of CO and water or CO_2, respectively. The resulting n-alkane has one carbon atom less than the original fatty acid [14].

The Ni- and Co-promoted molybdenum sulfide catalysts have been typically used in the hydrodeoxygenation of triglycerides, fatty acids, and esters [1, 3, 5, 11, 15-17]. The conventional metal sulfide catalysts, which are less expensive catalysts [18], showed high activity in the deoxygenation of triglycerides and model compounds; nevertheless, sulfur leaching lead to catalyst deactivation and sulfur contamination in the liquid products [19-22]. It should be noted that the metal sulfide catalysts require the addition of sulfiding agents e.g., CS_2 and DMDS, to the liquid feed to avoid catalyst deactivation during the deoxygenation reactions [13, 23]. Furthermore, the trace amount of water that is produced from the DCO and HDO reactions would hasten the sulfur leaching and rigorously shorten the lifetime of catalysts [24].

To develop the next generation of hydrodeoxygenation catalysts, the metal catalysts or sulfur-free catalysts in reduced states, such as Ni [2, 13, 16, 25-27], Co [13, 19], Pd [28-31], Pt [32], and Ru [33, 34], are good candidates for the deoxygenation reactions. Some metal catalysts, such as Ni, Pd, and Pt, are favorable in the DCO and DCO_2 pathways [35]. The hydrogen consumption for the deoxygenation of triglycerides/fatty acids/esters decreased in the order of HDO > DCO > DCO_2; thus the DCO and DCO_2 routes may be more theoretically economical than the HDO route [20, 21]. The noble metal catalysts imply an extremely high cost in green diesel production, thus limiting their use in the large-scale applications [2, 13]. Accordingly, the transition metal catalysts, such as Ni and Co, which also display a good catalytic activity, have been employed as great catalysts in the deoxygenation process. However, only a few studies have been reported on the deoxygenation of triglycerides. Peng *et al.* [20] investigated the catalytic deoxygenation of crude microalgae oil with a Ni/ZrO_2 catalyst in a trickle bed reactor at 543

K and 4 MPa. A 70 wt.% yield of *n*-heptadecane was obtained, and the catalyst did not significantly deactivate after 72 h-on stream. Kim *et al.* [36] reported the effect of temperature and pressure on the hydrotreating of soybean oil over a Ni/SiO_2-Al_2O_3 catalyst in batch and continuous flow reactors in the range of 573-713 K and 2.5 – 15 MPa. Stusentschnig and co-workers [4] hydrotreated the crude palm oil with the commercial Raney nickel catalyst at 633 K and 9 MPa in batch mode. After 5 h of reaction time, 100% conversion with alkanes yields of mainly *n*-heptadecane and *n*-octadecane between 54 and 60% were achieved. In addition, the mixed metal and metal oxide catalysts, e.g. Pt/Nb_2O_5[37] and $FeNi/SiO_2$[38], have been recently developed for deoxygenation. The unique performance of the mixed metal and metal oxide phases could be ascribable to their cooperation in which the H_2 is dissociated by metallic sites and carboxylic acid is adsorbed at the oxygen vacancy of metal oxide sites[37-38]. Nevertheless, to the best of our knowledge, the deactivation and regeneration in the hydrodeoxygenation reaction over metal catalysts has certainly not been reported in the literature. Consequently, the understanding of the deactivation and regeneration processes is important for improving and optimizing the process conditions.

In the present work, the deactivation behavior of Ni/γ-Al_2O_3 and Co/γ-Al_2O_3 catalysts in palm oil hydrodeoxygenation was studied in a continuous-flow trickle bed reactor at 573 K and 5 MPa over a reaction time of 150 h. Their catalytic performances were evaluated according to the triglyceride conversion, product yield, and the contribution of HDO (hydrodeoxygenation) and DCO_x (decarbonylation and/or decarboxylation), which were estimated based on the mole balance corresponding to the fatty acids in the oil feed. The calcined, prereduced, spent and regenerated catalysts were subsequently characterized to clarify the origin of deactivation and regeneration characteristics using a combination of techniques: temperature programmed reduction (TPR), N_2 sorption, CO pulse chemisorption, X-ray diffraction (XRD), X-ray absorption near edge structure (XANES), transmission

electron microscopy (TEM) and temperature programmed oxidation (TPO). Furthermore, the regenerability of the spent catalysts after the long-term tests was also reported.

2. Experimental

2.1 Catalyst preparations

The γ-Al_2O_3 support (1.8 mm diameter, Sasol Company, Germany, purity 99.9%) was crushed and sieved to 0.5 – 1.0 mm diameter. The Co and Ni supported on the γ-Al_2O_3 catalysts (10 wt % of Ni and Co loading) were prepared by the incipient wetness impregnation method using cobalt (II) nitrate hexahydrate [$(Co(NO_3)_2.6H_2O)$, Sigma-Aldrich, purity ≥98%] and nickel (II) nitrate hexahydrate [$(Ni(NO_3)_2.6H_2O)$, Sigma-Aldrich, purity 99.999%] as the corresponding metal salt precursors. After impregnation, the resultant samples were dried at 393 K for 12 h and then calcined at 773 K for 5 h.

2.2 Catalyst characterizations

Powder X-ray diffraction (XRD) patterns of the samples were collected on an X-ray diffractometer (D8 ADVANCE, Bruker, Ltd., Germany) using Cu Kα radiation. The measurement was operated at 40 kV and 40 mA in steps of 0.02^o s^{-1} with a step time of 0.5 s over the range of $20^o < 2\theta < 80^o$.

The X-ray absorption near edge structure (XANES) technique at Ni K-edge (8333 eV) and Co K-edge (7709 eV) were acquired at the SUT-NANOTEC-SLRI XAS Beamline (BL-5.2) of the Synchrotron Light Research Institute (Public Organization), Thailand using a double Ge (2 2 0) crystal monochromator for the selection of photon energy. The data were obtained at room temperature in the transmission mode using a 13-element Ge detector. The samples were pressed into a frame covered by polyimide tape before mounting to the sample holder. The NiO, Ni foil, Co_3O_4, CoO, and Co foil were used as the reference standards for

the XANES analysis. The XANES spectra by linear combination fitting were analyzed through the Athena program.

The specific surface area, total pore volume, and pore diameter of the samples were measured at 77 K with a nitrogen adsorption-desorption technique (Nova 2000e, Quantachrome Instruments, Germany). Prior to measurement, the samples were degassed at 393 K for 3 h. Pore size distributions of the samples were determined from the desorption branch of the isotherms using the Barrett-Joyner-Hallenda (BJH) method. The specific surface area was estimated based on the BET approach. The total pore volume was measured at the relative pressure (P/P_0) of 0.98.

The H_2 temperature programmed reduction (H_2-TPR) was carried out using a CHEMBET-Pulsar Quantachrome Instruments in a quartz U-tube reactor with 20 mg of sample. Prior to the experiments, the samples were pre-treated at 393 K for 1 h at a He flow rate of 30 cm^3/min. The reduction was conducted in a 5 vol % H_2/Ar flow rate of 30 cm^3/min at a heating rate of 10 K/min from 373 to 1273 K. The hydrogen consumption was analyzed using a thermal conductivity detector (TCD). The representative metallic sites of the catalysts were determined by CO pulse chemisorption experiments with the same apparatus as used for H_2-TPR. A 50 mg quantity of catalyst was reduced with a 5 vol% H_2/Ar flow rate of 30 cm^3/min at 973 K for 3 h. The pulses of CO (0.05 cm^3) were injected through the sample until CO saturation was attained. Temperature-programmed oxidation (TPO) combined with a mass spectroscopy detector was used to determine the amount of coke deposited on the spent catalyst using the same apparatus used for the H_2-TPR experiment. Prior to the TPO experiments, the spent catalyst samples (50 mg) were pre-treated at 673 K for 1 h under a He flow rate of 30 cm^3/min. The oxidation was conducted by raising the temperature from 373 to 1073 K at a heating rate of 10 K/min in a 5% O_2/He flow rate of 30

165 cm^3/min. The product gases were detected by online mass spectroscopy.

166 The morphology and particle size of the catalysts were examined by transmission
167 electron microscopy (TEM) at 200 kV on an FEI TECNAI G2-20S-TWIN instrument
168 equipped with an energy dispersive spectrum (EDS) analysis facility.

169 **2.3 Catalytic hydrodeoxygenation tests-durability evaluation**

170 Long-term durability reaction tests to investigate the deactivation and regeneration
171 behaviors were evaluated in a custom-made down-flow trickle-bed reactor with an internal
172 diameter of 7 mm, length of 210 mm, and a volume of 8 cm^3. The effect of external mass
173 transfer resistance in the catalyst bed was negligible under the working conditions as a further
174 increase in the space velocity with a fixed WHSV has no impact on the conversion and
175 product yield. The details of the reactor apparatus are presented elsewhere.[11] A palm oil
176 feedstock (a high purity refined palm olein type with a free fatty acid content <1 wt %) was
177 commercially obtained from a local market in Thailand. The fatty acid compositions of
178 refined palm olein (wt %), determined through the fatty acid methyl esters (FAMEs) obtained
179 from the transesterification of triglycerides with methanol using a base catalyst, were as
180 follows: lauric acid (C12:0) 0.4%; myristic acid (C14:0) 0.8%; palmitic acid (C16:0) 37.4%;
181 palmitoleic acid (C16:1) 0.2%; stearic acid (C18:0) 3.6%; oleic acid (C18:1) 45.8%; linoleic
182 acid (C18:2) 11.1%; linolemic acid (18:3) 0.3%; arachidic acid(C20:0) 0.3%; and eicosenoic
183 acid (C20:1) 0.1% [39]. The catalysts (5.5 g) were loaded into the reactor and then were *in situ*
184 prereduced with a flow of pure H_2 (200 cm^3/min, Praxair, purity 99.99%) at 773 K for 3 h. In
185 the reaction testing, the reactor was heated to the desired temperature and was pressurized
186 with H_2 to the desired pressure controlled by a back pressure regulator. An HPLC pump was
187 used to introduce the oil feed, and the H_2 feed was controlled by mass flow controllers. The
188 deactivation and regeneration experiments in the palm oil hydrodeoxygenation were

conducted at a temperature of 573 K, H_2 pressure of 5 MPa, liquid hourly space velocity (LHSV) of 1 h^{-1}, and a H_2/oil feed ratio of 1,000 N(cm^3/cm^3). Note that after a long-term reaction test was completed, the catalysts were cooled to room temperature under N_2 flow before exposition in air and being further characterized by various techniques. Furthermore, the regeneration experiments were conducted by calcination in air at 773 K for 5 h and reduction in H_2 at 773 K for 3 h.

2.4 Product analysis

After the separation of the water and oil-phase products obtained from the hydrodeoxygenation experiments, they were analyzed offline by a gas chromatography (GC) equipped with a capillary column (DB-1HT, 30 m × 0.32 mm × 0.1 μm) and a flame ionization detector (FID) (GC-2014, Shimadzu). The calibration curve of standards was used to quantify a composition of *n*-alkanes (*n*-C_8 to *n*-C_{18}) in the liquid products. Briefly, 50 mg of sample was diluted with 1 cm^3 of hexane and 0.001 cm^3 of sample was injected into the GC with a split ratio of 100. High injection and column temperatures were used to directly analyze the triglyceride without chemical derivatization [20, 40]. The injection and detector temperatures were 613 and 643 K, respectively. The temperature program was increased from 313 to 543 K at a rate of 8 K/min, and held for 11 min, followed by an increase of 15 K/min to 643 K, and held for 15 min. The composition of gas products (C_3H_8, C_2H_6, CH_4, CO, CO_2, and H_2) was analyzed by an online GC equipped with two packed columns (molecular sieve 5A and Porapak Q) and a thermal conductivity detector (TCD) (GC-14B, Shimadzu).

For an in-depth analysis of the catalyst performance evaluation, the mole balance of organic liquid products was used to determine the conversion and product yields; the mole balance was always above 95% for all conditions. The conversion was defined as the moles of reactants (triglyceride) converted to others (intermediates and hydrocarbons). The product

yields were theoretically determined based on the mole balance of *n*-alkanes in the product corresponding to the moles of fatty acids in the oil feed. The product yield of *n*-C_{15} to *n*-C_{18} fraction and conversion were calculated using the following equations:

$$\text{Conversion (\%)} = \left(\frac{\text{mole of triglycerides in feed} - \text{mole of triglycerides in product}}{\text{mole of triglycerides in feed}} \right) \times 100 \quad (1)$$

$$\text{Product yield (\%)} = \left(\frac{\text{Total mole of } n\text{–alkanes } (n\text{–}C_{15} \text{ to } n\text{–}C_{18}) \text{ in product}}{\text{Total mole of } C_{16} \text{ and } C_{18} \text{ fatty acid in feed}} \right) \times 100 \quad (2)$$

The relative activity of decarbonylation and decarboxylation reactions could not be directly correlated to the amount of CO and CO_2 detected in the gas phase due to the possible gas-phase reactions involved, such as methanation and water-gas shift reactions. Consequently, the percent contribution of hydrodeoxygenation (HDO) and combined decarbonylation and/or decarboxylation (DCO_x) reactions were also calculated based on the mole balance, using the total moles of *n*-alkanes with even numbers (HDO) or odd numbers (DCO_x) of carbon atoms in the liquid product, to the moles of fatty acids in the oil feed using the following equations:

$$\text{HDO (\%)} = \left(\frac{\text{Total mole of } n\text{–alkanes } (n\text{–}C_{16} \text{ and } n\text{–}C_{18}) \text{ in product}}{\text{Total mole of } C_{16} \text{ and } C_{18} \text{ fatty acid in feed}} \right) \times 100 \quad (3)$$

$$DCO_X \text{ (\%)} = \left(\frac{\text{Total mole of } n\text{–alkanes } (n\text{–}C_{15} \text{ and } n\text{–}C_{17}) \text{ in product}}{\text{Total mole of } C_{16} \text{ and } C_{18} \text{ fatty acid in feed}} \right) \times 100 \quad (4)$$

3. Results and discussions

3.1 Deactivation behaviors

The long-term reaction tests were performed for 150 h on-stream to examine the changes in the activity, performance, and selectivity of Ni/γ-Al_2O_3 and Co/γ-Al_2O_3 catalysts in the palm oil hydrodeoxygenation. The reaction conditions were as follows: reaction temperature = 573 K, H_2 pressure = 5 MPa, H_2/oil ratio = 1000 N(cm^3/cm^3), and LHSV = 1 h^{-1}. **Fig. 1** shows the triglyceride conversion and product yield on the catalytic performance of Ni/γ-Al_2O_3 and Co/γ-Al_2O_3 catalysts as a function of reaction time. It should be noted that the hydrodeoxygenation reaction over pure γ-Al_2O_3 resulted in 56% conversion of the triglyceride without a liquid alkane product yield. The results suggested that only saturated triglyceride scission to free fatty acids and propane occurred. Therefore, γ-Al_2O_3 played no catalytic role in the hydrodeoxygenation of the triglycerides. Interestingly, the product yield was achieved when the reaction was catalyzed by the metallic species, confirming the hydrodeoxygenation activity of the metallic sites of Ni or Co species. The triglyceride conversion, shown in **Fig. 1**, remained steady at ~100% throughout the 150 h reaction time during the test. Over the Ni catalyst, the product yield was generally between 85.7 – 94.4%, with an average value of 92.2 ± 2.2%. Meanwhile, over the Co catalyst, the product yield was also between 83.8 – 93.8% with an average value of 88.6 ± 3.6% at the first 100 h reaction time. Furthermore, the slight increase of product yield observed during the first 24-h reaction time was likely due to the formation of metallic Ni or Co by the *in situ* reduction during working conditions. As demonstrated in **Fig. 1**, at reaction times > 100 h, a decrease in product yield from 92.2 to 75.6% was observed over the Ni catalyst, whereas, a dramatic drop in product yield from 88.6% to ca. 56.6% could be noticed over the Co catalyst. These results indicated that the Ni and Co catalysts showed a significant catalyst deactivation over 100 h of reaction time. It should be noted that the catalytic activity on the palm oil

hydrodeoxygenation over the Ni catalyst seems to be greater than the Co catalyst. Furthermore, the percent deactivation of the catalysts was evaluated based on the product yield after 150 h compared with the average product yield during the first 100 h of reaction. The deactivation of the Ni and Co catalysts was 19.8% and 36.6%, respectively. It is clear that the Co catalyst was faster deactivated than the Ni one.

Although the triglyceride conversion remained constant throughout the 150 h reaction experiment, the changes in the liquid product properties were observed at reaction times in the range of 100-150 h (**Fig. 1**). The liquid product solidified at room temperature and was comprised of *n*-alkanes and oxygenated intermediates (i.e., free fatty acids, alcohols, and esters) including a small amount of triglycerides. This finding indicated that the Ni and Co metallic sites became deactivated and the reaction mainly proceeded through the hydrogenation of the C=C bonds in the unsaturated triglycerides, followed by C-O bond cleavage via the hydrogenolysis of the saturated triglyceride to produced free fatty acids and propane, indicating incomplete hydrodeoxygenation activity. The actual operation should avoid these conditions due to the strong adsorption of the oxygenated intermediates on the catalyst active sites, thus providing that the catalysts underwent rapid deactivation.

When the Ni was used, at 100 h of reaction time, DCO_x (decarbonylation, DCO and/or decarboxylation, DCO_2 pathways) (89.2 ± 2.4%) were a major reaction pathway, whereas, HDO, hydrodeoxygenation, (2.1 ± 0.3%) was a minor reaction pathway (**Fig. 2**). Interestingly, the dominant contribution over the Co catalyst during 100 h of reaction time was from both DCO_x (43.0 ± 3.3%) and HDO (45.8 ± 3.0%) pathways, suggesting that the triglycerides were deoxygenated through DCO, DCO_2, and HDO (**Fig. 2**). This finding indicated that the metallic sites of the Co catalyst were responsible for all three major reaction pathways, whereas, the metallic sites of Ni, strongly promoted DCO and/or DCO_2

reactions. The palm oil used in this study was mainly composed of C_{16} and C_{18} fatty acids (>98.4 wt %). Thus, the main composition of the liquid product was *n*-C_{15} and *n*-C_{17} due to highly selective DCO and DCO_2 reactions over the Ni catalyst (**Fig. 3**). On the contrary, *n*-C_{15}, *n*-C_{16}, *n*-C_{17}, and *n*-C_{18} were a major product composition when the Co catalysts were used (**Fig. 3**). Moreover, a small amount of light hydrocarbon compositions (*n*-C_8 to *n*-C_{14}) (results not shown) was observed during the hydrodeoxygenation, suggesting that the cracking reaction proceeded over the Ni and Co catalysts by C-C bond cleavage. It should be noted that the contribution and liquid product composition were also observed to change in similar way to that of the product yield.

The gas product compositions as a function of reaction time are represented in **Fig. 4**. When the Ni and Co catalysts were used, CH_4 was a major gas composition (≈20 mole % for Ni catalyst; ≈10 mole % for Co catalyst) as a result of the methanation reaction between CO or CO_2 with H_2, as well as the cracking reaction, implying that the metallic sites of the Ni and Co catalysts strongly promoted methanation and cracking reactions. The CO and CO_2 were not detected during the hydrodeoxygenation. When the reaction was catalyzed by Ni, the amount of C_3H_8 (< 1 mole %), produced by the hydrogenolysis of triglycerides, was lower than that of the Co catalyst, suggesting that the cracking reaction of C_3H_8 to C_2H_6 and CH_4 by C-C cleavage occurs over the Ni catalyst. Furthermore, the formation of the CH_4, C_2H_6, and C_3H_8 species in the gas product could be associated with the cracking reaction in the liquid phase. As seen in **Fig. 4**, the activity in the gas phase reactions (mainly methanation and cracking reactions) was not strongly affected as a function of time on stream over the Ni catalyst; nevertheless, the composition of gas product mainly CH_4, C_2H_6, and C_3H_8, slightly decreased after 80 h of reaction time over the Co catalyst. It should be deduced that the decay of the metallic sites of Ni catalyst showed a milder effect on the gas phase reactions.

306 **3.2 Catalyst characterizations**

307 In order to understand the deactivation and regeneration behaviors, as well as a reason
308 for the activity decline, in the Ni/γ-Al_2O_3 and Co/γ-Al_2O_3 catalysts used in the
309 hydrodeoxygenation, the calcined, prereduced, spent and regenerated catalysts were
310 characterized by temperature programmed reduction, N_2 sorption, CO pulse chemisorption,
311 X-ray diffraction, X-ray absorption near edge structure, transmission electron microscopy,
312 and temperature programmed oxidation.

313 The H_2-TPR experiments were conducted to investigate the reducibility of Ni/γ-
314 Al_2O_3 and Co/γ-Al_2O_3 catalysts, as well as to study the interaction between metal species and
315 γ-Al_2O_3 support in the catalysts (**Fig. 5)**. Firstly, the reduction peak of both pure NiO and
316 Co_3O_4 catalysts revealed a broad peak at approximately 750 K, indicating the nature of the
317 reduction behavior of the pure metal oxide. The reduction profile of Ni/γ-Al_2O_3 showed a
318 broad peak composed of three contributions (~943, ~1033, and ~1153 K), representing the
319 presence of different nickel species. The peak at 943 K was attributed to the reduction of bulk
320 NiO species to Ni^0, which have a weak interaction with the support. The second peak at 1033
321 K also represented the NiO species, which have stronger metal and support interactions, or
322 smaller particles located inside the pore. In addition, the reduction peak at the high
323 temperature of 1153 K could be assigned to stronger Ni and γ-Al_2O_3 interactions or nickel
324 aluminate phases with a spinel structure ($NiAl_2O_4$) [2, 26, 41]. On the other hand, the TPR profile
325 of Co/γ-Al_2O_3 showed a broad curve from 703 to 1073 K with three different peaks at ~793,
326 ~898, and ~1023 K. The transformation of Co_3O_4 to Co^0 occurred in two steps; the first peak,
327 at 703–823 K, was ascribed to the reduction of Co_3O_4 to CoO and the second one, at 823–953
328 K, to the subsequent reduction of CoO to Co^0. Additionally, the peak at higher temperature
329 (1023 K) may be assigned to the existence of a Co species with smaller crystallite sizes or
330 stronger metal-support interactions. [13, 42] Note that a high reduction temperature for catalyst

activation should be avoided due to the formation of large metal particle size and/or the transformation of γ-Al_2O_3 to other Al_2O_3 phases, thus providing the low activity and stability toward the reaction of catalysts. Therefore, the Ni and Co catalysts were *in situ* prereduced at a lower temperature (773 K) with pure H_2 for 3 h before catalytic hydrodeoxygenation testing.

To investigate possible changes in the catalyst texture, the BET specific surface area, total pore volume, and average pore diameter of bare γ-Al_2O_3, prereduced, spent, and regenerated catalysts are summarized in **Table 1.** The surface area of bare γ-Al_2O_3 was 201.1 m^2/g with a total pore volume of 0.55 cm^3/g. The BET surface area and pore volume typically decreased by 10% after metal loading. The decrease of the specific surface area and total pore volume of the catalysts would be due to the metal converging on the γ-Al_2O_3 support and blockage of the pores by metal species. Interestingly, the observed pore sizes of all the catalysts were approximately 7.5 nm and did not change significantly after metal loading in the range studied. N_2 adsorption–desorption isotherms (results not shown) of γ-Al_2O_3 and the catalysts exhibited type-IV isotherms, a typical characteristic of a mesoporous structure. As seen in **Table 1**, the BET surface area of prereduced Ni/γ-Al_2O_3 did not significantly differ when compared with the calcined catalysts; whereas, the surface area of pre-reduced Co/γ-Al_2O_3 catalysts was somewhat less than that of the calcined catalysts. This may be due to the sintering of cobalt particles during H_2 reduction at 773 K. A significant decrease in BET surface area, pore volume, and pore diameter was observed from both spent Ni/γ-Al_2O_3 and Co/γ-Al_2O_3 catalysts after 150 h on-stream. It should be noted that the changes in the physical structural properties of the spent catalyst were possibly caused by carbonaceous deposits on the pore channels and/or external surface of catalysts, thus leading to pore blocking. In addition, the pore blocking could result in catalyst deactivation due to limiting diffusion of the reactants or intermediates and the products dispersion from the catalysts active sites [43, 44].

However, the texture properties of the catalysts after regeneration by calcining in air at 773 K for 5 h were similar to the prereduced catalysts, indicating that the carbon deposited on the catalyst was completely removed, and the pore structure did not change under the hydrodeoxygenation experiments.

CO uptake, which represents a number of active sites on a catalyst, was used to elucidate the loss of catalyst active sites (**Table 1)**. The CO uptake of Ni/γ-Al_2O_3 was typically higher than that of Co/γ-Al_2O_3. It should be confirmed that the decrease in catalyst active sites after a 150 h experiment was likely due to the coking or catalyst sintering. Furthermore, the increase in the CO uptake after regeneration may be due to the redispersion of the Ni and Co species during the carbon burning.

The phase identity and crystallinity of the calcined, prereduced, spent, and regenerated catalysts were revealed through XRD patterns (**Figs. 6 and 7**). Three peaks at 2θ=37.5°, 46° and 67° assigned to the γ-Al_2O_3 phase with low crystallinity were observed for all catalysts [45]. The calcined Ni/γ-Al_2O_3 catalyst (**Fig. 6, pattern a)** exhibited three diffraction peaks at 2θ=37.4°, 44°, and 63° which correspond to NiO (111), NiO (200), and NiO (220), respectively, which approximately disappeared after pre-reduction in pure H_2 at 500 °C (**Fig. 6, pattern b**) [21]. The diffraction peak of metallic Ni at 2θ=44.6°, 52.2°, and 76.5° could be attributed to the reflection of (111), (200), and (220) planes, respectively [46]. As represented in **Fig. 7, pattern a**, the diffraction peaks at 2θ=31.3°, 37.7°, 59.5° and 65.4°, which were seen in calcined Co/γ-Al_2O_3 catalysts, were assigned to those of spinel Co_3O_4; meanwhile, the pre-reduced catalyst (**Fig. 7, pattern b**) exhibited a diffraction peak for CoO at 2θ=37.2° and metallic Co at 2θ=44.2° and 52.3°.[47] The XRD patterns of the catalysts after the hydrodeoxygenation reaction, shown in **Figs. 6, pattern c and 7, pattern c**, revealed the increase in the intensity of the diffraction peak of metallic Ni and Co peaks, indicating that

the crystallinity size of the Ni and Co crystallites slightly increased. Thus, the phenomena implied that metallic Ni and Co particles start to aggregate during the 150 h hydrodeoxygenation reaction experiment. Additionally, the XRD patterns of regenerated Ni and Co by calcining in air at 500 °C for 5 h (**Figs. 6, pattern d and 7, pattern d**) illustrated that the regenerated catalysts exhibit crystalline structures of NiO and Co_3O_4 for the regenerated Ni and Co catalysts, respectively. Generally, in the hydrodeoxygenation reaction, a water content of 10-15 wt % was found in the liquid product. The transformation of γ-Al_2O_3 into γ-AlOOH in the presence of water under hydrothermal conditions has been reported by some researchers [48, 49]. As demonstrated in the XRD patterns of the catalysts after reaction, the transformation of γ-Al_2O_3 into γ-AlOOH did not occur during 150 h on-stream. The γ-Al_2O_3 has been stabilized in the presence of the palm oil, alkanes, oxygenated intermediates, and water products under the working conditions.

The fist-row transition metal elements revealed well-defined site symmetry spectra in the X-ray absorption near edge structure (XANES) characteristics [50, 51]. Normalized Ni and Co K-edge XANES spectra of the calcined, prereduced, and spent Ni/γ-Al_2O_3 and Co/γ-Al_2O_3 catalysts are displayed in **Figs. 8** and **9**, respectively. The standard edge energy was calibrated at the first inflection point in the metal foil calibration spectrum (8333.0 eV for Ni, 7709.0 eV for Co) as reported in the literature [50, 52]. The intensity of the pre-edge peak and white line was used to consider the main features, reflecting the oxidation state of the Ni and Co catalysts on the γ-Al_2O_3 support. Firstly, the shape and features of the calcined Ni (**Fig. 8**) and Co (**Fig. 9**) catalysts were similar to the spectra of NiO and Co_3O_4 spinel, respectively, indicating that the samples were in the form of NiO and Co_3O_4 on the γ-Al_2O_3 support, which was consistent with the XRD patterns. In the case of the Ni catalysts, shown in **Fig. 8**, after being prereduced and tested in the hydrodeoxygenation, the edge energy of the prereduced and spent Ni catalysts shifted to that of Ni foil and the intensity of the white line decreased,

405 whereas the pre-edge increased. This suggested that the NiO on the γ-Al_2O_3 species were not
406 completely reduced so oxides of Ni existed. In the case of the Co catalysts **(Fig. 9)**, it is clear
407 from the XANES data that it is easy to distinguish between metallic Co, CoO, and Co_3O_4
408 phases. After being prereduced, the edge energy of the prereduced Co catalyst shifted to that
409 of CoO, whereas the intensity of the line decreased and the pre-edge increased when CoO
410 species transformed into Co metallic species were observed. The transformation of Co_3O_4 to
411 Co^0 occurred in two steps: the first step, the transition of Co_3O_4 to CoO and the second one,
412 the reduction of CoO to Co^0, which is consistent with what was observed in the TPR
413 experiments.

414 To quantify the amount of Ni and Co species in the prereduced, calcined and spent
415 catalysts, a linear combination fit (LCF) of the XANES spectra was applied and performed
416 using the XANES data of standard materials (NiO and Ni foil for Ni; Co_3O_4, CoO, and Co
417 foil for Co) as possible compositions. This procedure yielded the percentage of the catalyst
418 species on the γ-Al_2O_3 support**.** The weight percentages are summarized in **Table 3** for the Ni
419 and Co species. The statistical goodness-of-fit parameter with R-factor (coefficient of
420 determination) shows that the fit is reasonably good. The LCF confirmed that the NiO and
421 Co_3O_4 species are the dominant metal phases in the calcined Ni/γ-Al_2O_3 and Co/γ-Al_2O_3
422 catalysts, respectively. After being prereduced, some of the NiO species were transformed to
423 metallic Ni, whereas, the Co_3O_4 species were first transformed to CoO before being
424 transformed to metallic Co. It is evident from the XANES data that the nickel oxide and
425 cobalt oxide were not completely reduced to the metallic form at 773 K for 3 h in the
426 presence of pure H_2. In addition, it could be observed that the amount of metallic Ni and Co
427 increased with an increase in the reaction time, indicating that the reduction continued to
428 occur during the hydrotreating process.
429

The combined XRD and XANES data confirmed that the nickel and cobalt oxides were not completely reduced to metallic phases. To confirm the role of metal oxides, the effect of prereduction temperature was conducted over Ni/γ-Al_2O_3 catalysts. As demonstrated in **Fig S1**, the metal oxide catalyst without prereduction exhibited much lower activity than that with prereduction. The result suggested that the metallic phase was the dominant active site for the reaction. In addition, the HDO activity remained almost constant, although the ratio of metal to metal oxide would change during the time course of reaction, especially the first few days. Therefore the role of metal oxide was not significant in the present HDO experiments. It should be noted that the increase in reduction temperature from 773 to 973 K to completely reduce the NiO phase drastically suppressed the catalytic activity due to the aggregation of metal particles.

To investigate the metal particle growth or sintering effect on the palm oil hydrodeoxygenation activity, typical TEM images and particle size distribution of prereduced, spent, and regenerated Ni and Co catalysts are represented in **Figs. 10 and 11**. The TEM images of the Ni catalysts (**Fig. 10**) display an uneven metal particle size, whereas, a less clear distinction between the metal and alumina was observed in TEM images of the Co catalysts (**Fig. 11**). Nonetheless, the most aggregation of Co particles could be distinguished due to the darkest contrast. The Co particles were less dispersed on the γ-Al_2O_3 support than the Ni particles, and most of the Co particles were clustered into large particles. The average particle size of the Ni and Co catalysts after the reaction somewhat increased from 10.7 ± 2.3 to 12.7 ± 2.1 nm and from 11.8 ± 3.9 to 12.2 ± 4.9 nm, respectively. This finding indicated that the average metal particle size increased slightly after the reaction, suggesting that the metal sintering occurred during the hydrodeoxygenation reaction. Furthermore, it should be noted that the metal particle sizes of the Ni and Co were much larger than the pore size of γ-Al_2O_3, suggesting that most particles would be located outside

the pore of alumina. Interestingly, the TEM images of the catalysts regenerated at 773 K in air for 5 h, followed by prereduction in H_2 at 773 K for 3 h also showed that the metal particles size of Ni and Co were 12.5 ± 2.4 and 10.5 ± 3.5, respectively. The particle size was not significantly changed before and after the regeneration under the thermal treatment. It should be deduced that the sintering may not be the main reason for catalyst deactivation because the reaction temperature 573 K was significantly lower than the melting point of the Ni and Co catalysts. The combination data of the XRD and TEM analyses showed the catalyst sintering was a reason for the catalyst deactivation during the palm oil hydrodeoxygenation. Note that the average metal particle size was measured from 50-100 particles to ensure a significant population variance.

Furthermore, the pre-reduced, spent, and regenerated Ni and Co catalysts were characterized by FE-SEM. As shown in **Fig. S2**, the morphology of the catalysts did not obviously change after the deoxygenation for 150 h and the regeneration process. Meanwhile, the elemental mapping analysis for the pre-reduced, spent, and regenerated Ni and Co catalysts (**Fig. S3**) based on SEM-EDX analysis revealed that distribution of the Ni species on the γ-Al_2O_3 support was more uniform than that of Co species. The agglomeration of some Ni species in the spent catalyst was observed which was consistent to the particles size of the spent Ni catalysts based on the TEM analysis.

The amount of carbonaceous species deposited on the spent catalysts was determined by temperature-programmed oxidation. The desorption curves of CO_2 measured by mass spectrometry, shown in **Fig. 12**, indicated that a large amount of CO_2 was released from the spent catalysts. According to the literature, the peaks at low temperature approximately 573 K correspond to more reactive amorphous carbon which adsorbed on the metallic sites; meanwhile, the oxidation of crystalline or graphitic carbon occurs at temperatures above 773

K [53-55]. The TPO profile of the spent Ni and Co catalysts showed a wide peak in the temperature range of 573–913 K with a peak maximum at ca. 813 K and ca. 763 K, respectively. The carbonaceous species deposited during hydrodeoxygenation could be removed above 773 K, suggesting that the formed carbon species were both amorphous and graphitic carbons. As summarized in **Table 3**, the carbon content of the spent Ni and Co was determined to be 34.88 mg/g_{cat} and 49.51 mg/g_{cat}, respectively; whereas, only trace amounts were detected in regenerated catalysts. It should be confirmed that the Co catalyst deactivated faster than the Ni catalysts due to the higher carbon formation rate on the catalyst surface. Thus TPO analysis indicated carbon deposition was a main cause for the catalysts' deactivation.

3.3 Regeneration behaviors

After the 150 h on-stream experiment, the product yield decreased from 92.2 to ca. 75.6% over the Ni catalyst and from 88.6% to ca. 56.6% over the Co catalyst. As discussed above, the major reason for catalyst deactivation was caused by the formation of carbonaceous species on the catalyst, and the minor reason was likely the partial sintering of the metal particles. At first, to find out the suitable temperature for the effective removal of the carbonaceous species, TGA (results not shown) was investigated in the range of 473-1073 K in the presence of air. The complete decomposition of carbon was observed at the temperature of 773 K, suggesting that the appropriate regeneration temperature was 773 K. Therefore, the spent catalysts after 150 h on-stream were regenerated by calcining at 773 K for 5 h. A higher regeneration temperature should be avoided due to the formation of large metal particle sizes, and the transformation of Ni and Co on γ-Al_2O_3 to metal aluminate phases. After regeneration, the catalysts exhibited the crystalline structures of metal oxide phases, which implied that the pre-reduction under H_2 at 773 K for 3 h was necessary. It should be deduced that the physical and chemical properties such as BET surface area, pore

volume, pore diameter, and metal particles size were not significantly different after the regeneration as shown in **Figs. 1-4,** indicating that the catalytic performance can be essentially restored after the regeneration. This suggests that the carbon deposited on the catalyst surfaces was completely removed and was the origin of the deactivation.

4. Conclusions

The deactivation and regeneration behaviors of the Ni/γ-Al_2O_3 and Co/γ-Al_2O_3 catalysts during palm oil hydrodeoxygenation in a trickle bed reactor have been studied and the concluding remarks are as follows:

- On the hydrodeoxygenation reaction test for 150 h, the Ni/γ-Al_2O_3 and Co/γ-Al_2O_3 catalysts exhibited good catalytic activity and stable performance for 100 h on-stream under the reaction conditions of temperature = 573 K, H_2 pressure = 5 MPa, H_2/oil ratio = 1000 N(cm^3/cm^3), and LHSV = 1 h^{-1}.
- After 100 h on-stream, the catalyst activity over the Ni catalyst gradually dropped; whereas, a dramatic decline can be observed over Co catalysts. According to the characterization data, the carbonaceous species deposited on the catalysts seemed to be the main cause of catalyst deactivation, and metal particle size growth was deduced to be the minor reason.
- The spent catalyst can be fully regenerated by calcination in air at a temperature of 773 K for 5 h, followed by prereduction in H_2 at 773 K for 3 h, resulting in a complete recovery of the catalytic performance.

Acknowledgements

The authors acknowledge the financial support from the National Nanotechnology

Center (NANOTEC), NSTDA, Thailand, the Thailand Research Fund (TRF) to K.F. (RSA5580055) and S.A., and the Thailand Graduate Institute of Science and Technology (TGIST) (Grant No. TG-55-09-54-004D) to A.S.

References

1 I. V. Deliy, E. N. Vlasova, A. L. Nuzhdin, E. Y. Gerasimov and G. A. Bukhtiyarova, *RSC Adv.*, 2014, **4**, 2242-2250.

2 P. Kumar, S. R. Yenumala, S. K. Maity and D. Shee, *Appl. Catal., A*, 2014, **471**, 28-38.

3 D. Kubička and L. Kaluža, *Appl. Catal., A*, 2010, **372**, 199-208.

4 A. F. H. Studentschnig, S. Schober and M. Mittelbach, *Energy Fuels*, 2013, **27**, 7480-7484.

5 Y. Liu, R. Sotelo-Boyás, K. Murata, T. Minowa and K. Sakanishi, *Energy Fuels*, 2011, **25**, 4675-4685.

6 C. Wang, Z. Tian, L. Wang, R. Xu, Q. Liu, W. Qu, H. Ma and B. Wang, *ChemSusChem*, 2012, **5**, 1974-1983.

7 T. V. Choudhary and C. B. Phillips, *Appl. Catal., A*, 2011, **397**, 1-12.

8 B. Donnis, R. G. Egeberg, P. Blom and K. G. Knudsen, *Top. Catal.*, 2009, **52**, 229-240.

9 H. Zhang, H. Lin, W. Wang, Y. Zheng and P. Hu, *Appl. Catal., B*, 2014, **150-151**, 238-248.

10 D. Kubička, J. Horáček, M. Setnička, R. Bulánek, A. Zukal and I. Kubičková, *Appl. Catal., B*, 2014, **145**, 101-107.

11 A. Srifa, K. Faungnawakij, V. Itthibenchapong, N. Viriya-empikul, T. Charinpanitkul and S. Assabumrungrat, *Bioresour. Technol.*, 2014, **158**, 81-90.

12 K. Faungnawakij and K. Suriye, in *New and Future Developments in Catalysis*, ed. S. L. Suib, Elsevier, Amsterdam, 2013, pp. 79-104.

13 C. Ochoa-Hernández, Y. Yang, P. Pizarro, V. A. de la Peña O'Shea, J. M. Coronado and D. P. Serrano, *Catal. Today*, 2013, **210**, 81-88.

14 S. Gong, A. Shinozaki, M. Shi and E. W. Qian, *Energy Fuels*, 2012, **26**, 2394-2399.

15 P. Priecel, D. Kubička, L. Čapek, Z. Bastl and P. Ryšánek, *Appl. Catal., A*, 2011, **397**, 127-137.

16 B. Veriansyah, J. Y. Han, S. K. Kim, S.-A. Hong, Y. J. Kim, J. S. Lim, Y.-W. Shu, S.-G. Oh and J. Kim, *Fuel*, 2012, **94**, 578-585.

17 H. Wang, S. Yan, S. O. Salley and K. Y. Simon Ng, *Fuel*, 2013, **111**, 81-87.

18 S. A. W. Hollak, R. W. Gosselink, D. S. van Es and J. H. Bitter, *ACS Catal.*, 2013, **3**, 2837-2844.

19 Q. Liu, Y. Bie, S. Qiu, Q. Zhang, J. Sainio, T. Wang, L. Ma and J. Lehtonen, *Appl. Catal., B*, 2014, **147**, 236-245.

20 B. Peng, X. Yuan, C. Zhao and J. A. Lercher, *J. Am. Chem. Soc.*, 2012, **134**, 9400-9405.

21 B. Peng, C. Zhao, S. Kasakov, S. Foraita and J. A. Lercher, *Chemistry*, 2013, **19**, 4732-4741.

22 B. Peng, Y. Yao, C. Zhao and J. A. Lercher, *Angew. Chem.*, 2012, **51**, 2072-2075.

23 J. Chen, H. Shi, L. Li and K. Li, *Appl. Catal., B*, 2014, **144**, 870-884.

24 C. Zhao, T. Brück and J. A. Lercher, *Green Chem.*, 2013, **15**, 1720.

25 E. Santillan-Jimenez, T. Morgan, J. Lacny, S. Mohapatra and M. Crocker, *Fuel*, 2013, **103**, 1010-1017.

26 H. Zuo, Q. Liu, T. Wang, L. Ma, Q. Zhang and Q. Zhang, *Energy Fuels*, 2012, **26**, 3747-3755.

27 R. Kaewmeesri, A. Srifa, V. Itthibenchapong and K. Faungnawakij, *Energy Fuels*, 2014.

28 J. Duan, J. Han, H. Sun, P. Chen, H. Lou and X. Zheng, *Catal. Commun.*, 2012, **17**, 76-80.

29 I. Simakova, O. Simakova, P. Mäki-Arvela, A. Simakov, M. Estrada and D. Y. Murzin, *Appl. Catal., A*, 2009, **355**, 100-108.

30 P. i. Mäki-Arvela, B. Rozmysłowicz, S. Lestari, O. Simakova, K. Eränen, T. Salmi and D. Y. Murzin, *Energy Fuels*, 2011, **25**, 2815-2825.

31 W. Kiatkittipong, S. Phimsen, K. Kiatkittipong, S. Wongsakulphasatch, N. Laosiripojana and S. Assabumrungrat, *Fuel Process. Technol.*, 2013, **116**, 16-26.

32 X. Kong, G. Wang, X. Du, L. Lu, L. Li and L. Chen, *Catal. Commun.*, 2012, **27**, 26-29.

33 L. Chen, Y. Zhu, H. Zheng, C. Zhang and Y. Li, *Appl. Catal., A*, 2012, **411-412**, 95-104.

34 L. Chen, Y. Zhu, H. Zheng, C. Zhang, B. Zhang and Y. Li, *J. Mol. Catal. A: Chem.*, 2011, **351**, 217-227.

35 A. Srifa, K. Faungnawakij, V. Itthibenchapong and S. Assabumrungrat, *Chem. Eng. J.*.

36 S. K. Kim, S. Brand, H.-s. Lee, Y. Kim and J. Kim, *Chem. Eng. J.*, 2013, **228**, 114-123.

37 K. Kon, W. Onodera, S. Takakusagi and K.-i. Shimizu, *Catal. Sci. Technol.*, 2014, **4**, 3705-3712.

38 X. Yu, J. Chen and T. Ren, *RSC Adv.*, 2014, **4**, 46427-46436.

39 N. Viriya-empikul, P. Krasae, W. Nualpaeng, B. Yoosuk and K. Faungnawakij, *Fuel*, 2012, **92**, 239-244.

40 M. Anand and A. K. Sinha, *Bioresour. Technol.*, 2012, **126**, 148-155.

41 D. Hu, J. Gao, Y. Ping, L. Jia, P. Gunawan, Z. Zhong, G. Xu, F. Gu and F. Su, *Ind. Eng. Chem. Res.*, 2012, **51**, 4875-4886.

42 Z. Ferencz, K. Baán, A. Oszkó, Z. Kónya, T. Kecskés and A. Erdőhelyi, *Catal. Today*, 2013.

43 C. H. Bartholomew, *Appl. Catal., A*, 2001, **212**, 17-60.

44 X. Lin, Y. Fan, G. Shi, H. Liu and X. Bao, *Energy Fuels*, 2007, **21**, 2517-2524.

45 P. Hirunsit, K. Faungnawakij, S. Namuangruk and C. Luadthong, *Appl. Catal., A*, 2013, **460-461**, 99-105.

46 Y. Wang, G. Luo, X. Xu and J. Xia, *Catal. Commun.*, 2014, **57**, 83-88.

47 S.-M. Kim, J. W. Bae, Y.-J. Lee and K.-W. Jun, *Catal. Commun.*, 2008, **9**, 2269-2273.

48 J. G. Dickinson and P. E. Savage, *ACS Catal.*, 2014, **4**, 2605-2615.

49 M. El Doukkali, A. Iriondo, J. F. Cambra, I. Gandarias, L. Jalowiecki-Duhamel, F. Dumeignil and P. L. Arias, *Appl. Catal., A*, 2014, **472**, 80-91.

50 S. Lee, G. Keskar, C. Liu, W. R. Schwartz, C. S. McEnally, J.-Y. Kim, L. D. Pfefferle and G. L. Haller, *Appl. Catal., B*, 2012, **111–112**, 157-164.

51 Y. Yang, S. Lim, G. Du, Y. Chen, D. Ciuparu and G. L. Haller, *J. Phy. Chem. B*, 2005, **109**, 13237-13246.

52 P. Khemthong, W. Klysubun, S. Prayoonpokarach and J. Wittayakun, *Mater. Chem. Phy.*, 2010, **121**, 131-137.

53 P. Djinović, I. G. Osojnik Črnivec, B. Erjavec and A. Pintar, *Appl. Catal., B*, 2012, **125**, 259-270.

54 P. Wang, E. Tanabe, K. Ito, J. Jia, H. Morioka, T. Shishido and K. Takehira, *Appl. Catal., A*, 2002, **231**, 35-44.

55 J. Vicente, C. Montero, J. Ereña, M. J. Azkoiti, J. Bilbao and A. G. Gayubo, *Int. J. Hydrogen Energy*, 2014, **39**, 12586-12596.

Figure captions

Fig. 1. Triglyceride conversion and product yield over time on stream during palm oil hydrodeoxygenation on the catalytic performance and regeneration of the Ni/γ-Al_2O_3 and Co/γ-Al_2O_3 catalysts. Reaction conditions: 573 K, 5 MPa, LHSV of 1 h^{-1}, and H_2/oil ratio of 1,000 N(cm^3/cm^3)

Fig. 2. Contribution of HDO and DCO_x over time on stream during palm oil hydrodeoxygenation on the catalytic performance and regeneration of the Ni/γ-Al_2O_3 and Co/γ-Al_2O_3 catalysts. Reaction conditions: 573 K, 5 MPa, LHSV of 1 h^{-1}, and H_2/oil ratio of 1,000 N(cm^3/cm^3)

Fig. 3. Liquid product composition over time on stream during palm oil hydrodeoxygenation on the catalytic performance and regeneration of the Ni/γ-Al_2O_3 and Co/γ-Al_2O_3 catalysts. Reaction conditions: 573 K, 5 MPa, LHSV of 1 h^{-1}, and H_2/oil ratio of 1,000 N(cm^3/cm^3)

Fig. 4. Gas product composition over time on stream during palm oil hydrodeoxygenation on the catalytic performance and regeneration of the Ni/γ-Al_2O_3 and Co/γ-Al_2O_3 catalysts. Reaction conditions: 573 K, 5 MPa, LHSV of 1 h^{-1}, and H_2/oil ratio of 1,000 N(cm^3/cm^3)

Fig. 5. H_2-TPR profiles of the catalysts, (a) Ni/γ-Al_2O_3, (b) Co/γ-Al_2O_3, (c) NiO, (d) Co_3O_4

Fig. 6. XRD patterns of the (a) calcined, (b) prereduced, (c) spent, and (d) regenerated of Ni/γ-Al_2O_3 catalysts.

Fig. 7. XRD patterns of the (a) calcined, (b) prereduced, (c) spent, and (d) regenerated of Co/γ-Al_2O_3 catalysts.

Fig. 8. Normalized Ni K-edge XANES spectra of the calcined, prereduced, and spent Ni catalysts and the reference standards.

Fig. 9. Normalized Co K-edge XANES spectra of the calcined, prereduced, and spent Co catalysts and the reference standards.

Fig. 10. TEM images of the (a) prereduced, (b) spent, and (c) regenerated Ni/γ-Al_2O_3 and the particle size distribution of the (d) prereduced, (e) spent, and (f) regenerated Ni/γ-Al_2O_3.

Fig. 11. TEM images of the (a) prereduced, (b) spent, and (c) regenerated Co/γ-Al_2O_3 and the particle size distribution of the (d) prereduced, (e) spent, and (f) regenerated Co/γ-Al_2O_3.

Fig. 12. Temperature programmed oxidation profiles of the Ni/γ-Al_2O_3 and Co/γ-Al_2O_3 catalysts after 150 h on-stream.

660 **Table 1** Physicochemical properties of the calcined, prereduced, spent, and regenerated catalysts

Catalyst	Metal content[a] (wt.%)	S_{BET}[b] (m^2/g)	Total pore volume[c] (cm^3/g)	Pore diameter (BJH)[d] (nm)	CO uptake (umol/g)
γ-Al_2O_3	-	201.1	0.549	7.53	-
Calcined Ni/γ-Al_2O_3	9.42	178.1	0.454	7.51	-
Prereduced Ni/γ-Al_2O_3	-	177.2	0.497	7.51	26.5
Spent Ni/γ-Al_2O_3	-	105.1	0.236	5.44	18.7
Regenerated Ni/γ-Al_2O_3	-	178.6	0.519	7.51	32.5
Calcined Co/γ-Al_2O_3	9.05	181.2	0.470	7.51	-
Prereduced Co/γ-Al_2O_3	-	172.7	0.469	7.51	9.4
Spent Co/γ-Al_2O_3	-	100.8	0.239	5.44	0
Regenerated Co/γ-Al_2O_3	-	171.8	0.502	7.51	12.6

661

662 [a] Metal content determined by ICP-OES

663 [b] BET surface area calculated from the adsorption branch of the N_2 isotherm

664 [c] Total pore volumes calculated from the N_2 adsorption at a relative pressure of 0.98

665 [d] Pore diameter calculated from the desorption branch using the BJH method

666

667

668

669 **Table 2** Phase compositions obtained from linear combination fitting of the XANES spectra of the Ni and Co catalysts.

670

		Phase composition (wt %)				
Catalyst	R-factor*	Ni	NiO	Co	CoO	Co_3O_4
Calcined Ni/γ-Al_2O_3	0.01605	0.3	99.7	-	-	-
Prereduced Ni/γ-Al_2O_3	0.00522	31.7	68.3	-	-	-
Spent Ni/γ-Al_2O_3	0.00575	45.5	54.5	-	-	-
Calcined Co/γ-Al_2O_3	0.00721	-	-	0	4.9	95.1
Prereduced Co/γ-Al_2O_3	0.00899	-	-	22.7	74.6	2.7
Spent Co/γ-Al_2O_3	0.00395	-	-	67.7	32.3	0

671

672 * R-factor (coefficient of determination) is the statistical goodness-of-fit parameter

Table 3 Total coke contents before and after regeneration by calcining in air at 773 K for 5 h as obtained from temperature programmed oxidation

Catalysts	Carbon amount remained after the reaction (mg/g_{cat})	Carbon amount remained after the regeneration (mg/g_{cat})	Carbon amount removed after the regeneration (%)
Spent $Ni/\gamma\text{-}Al_2O_3$	34.88	0.02	99.94
Spent $Co/\gamma\text{-}Al_2O_3$	49.51	0.02	99.95

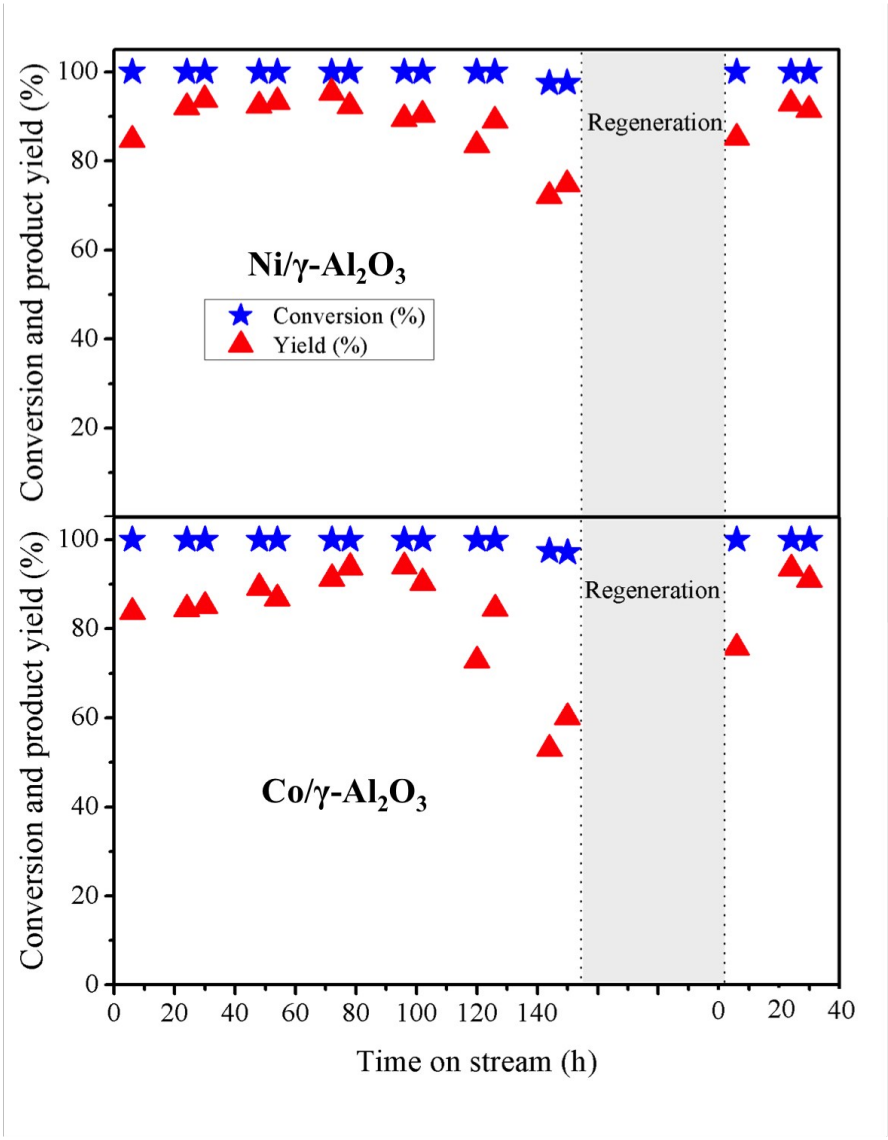

Fig. 1. Triglyceride conversion and product yield over time on stream during palm oil hydrodeoxygenation on the catalytic performance and regeneration of the Ni/γ-Al_2O_3 and Co/γ-Al_2O_3 catalysts. Reaction conditions: 573 K, 5 MPa, LHSV of 1 h^{-1}, and H_2/oil ratio of 1,000 N(cm^3/cm^3)

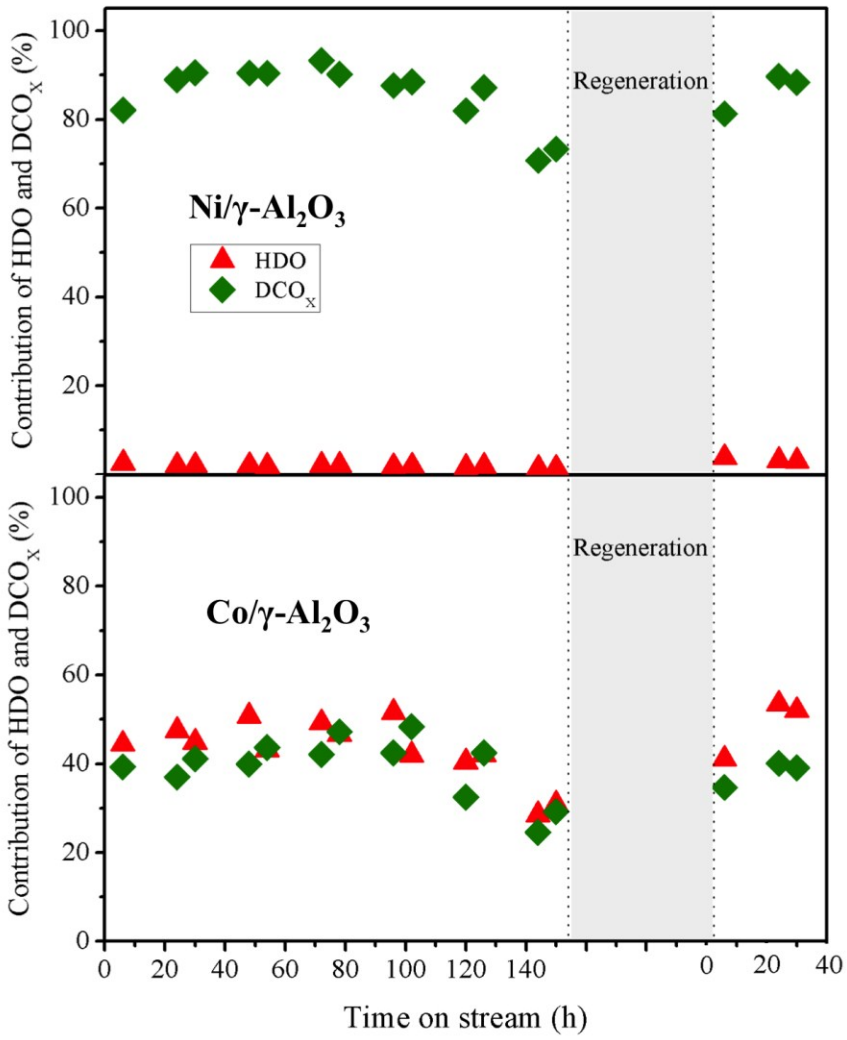

Fig. 2. Contribution of HDO and DCO_x over time on stream during palm oil hydrodeoxygenation on the catalytic performance and regeneration of the Ni/γ-Al_2O_3 and Co/γ-Al_2O_3 catalysts. Reaction conditions: 573 K, 5 MPa, LHSV of 1 h^{-1}, and H_2/oil ratio of 1,000 N(cm^3/cm^3)

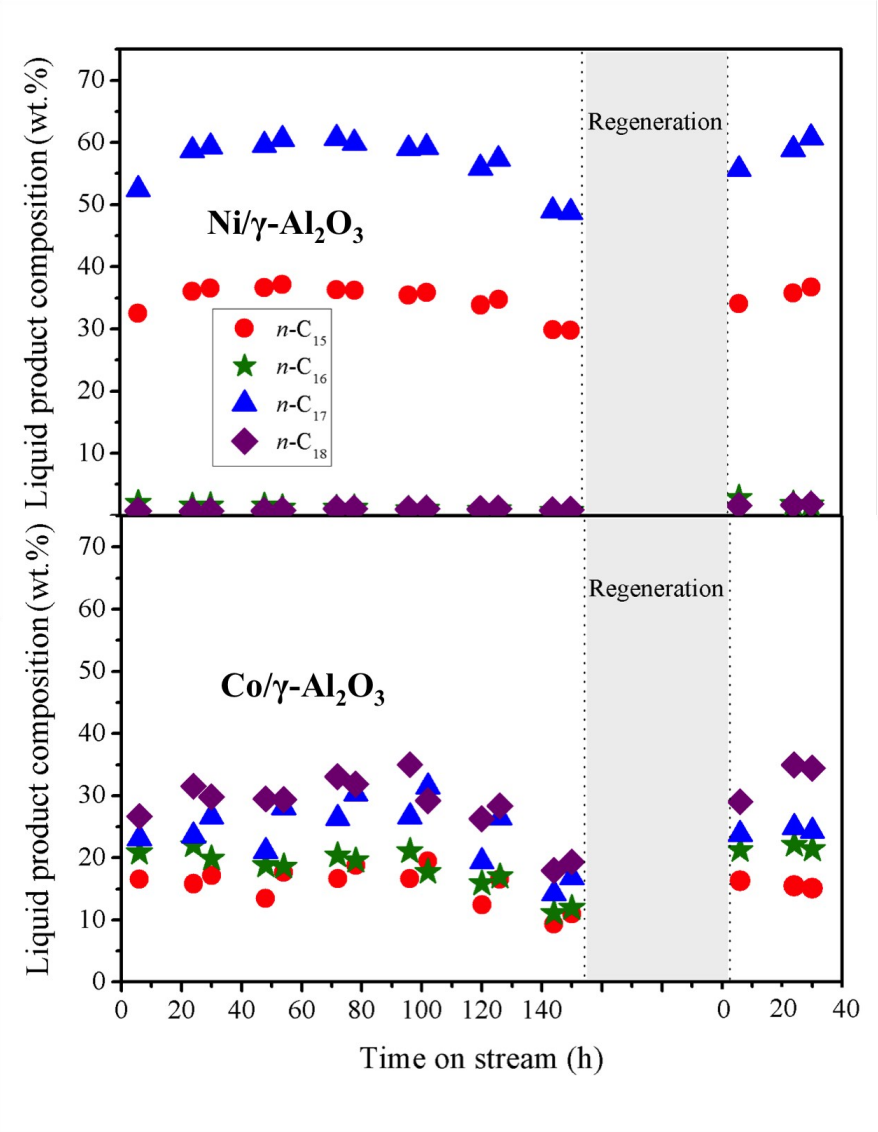

Fig. 3. Liquid product composition over time on stream during palm oil hydrodeoxygenation on the catalytic performance and regeneration of the Ni/γ-Al_2O_3 and Co/γ-Al_2O_3 catalysts. Reaction conditions: 573 K, 5 MPa, LHSV of 1 h^{-1}, and H_2/oil ratio of 1,000 N(cm^3/cm^3)

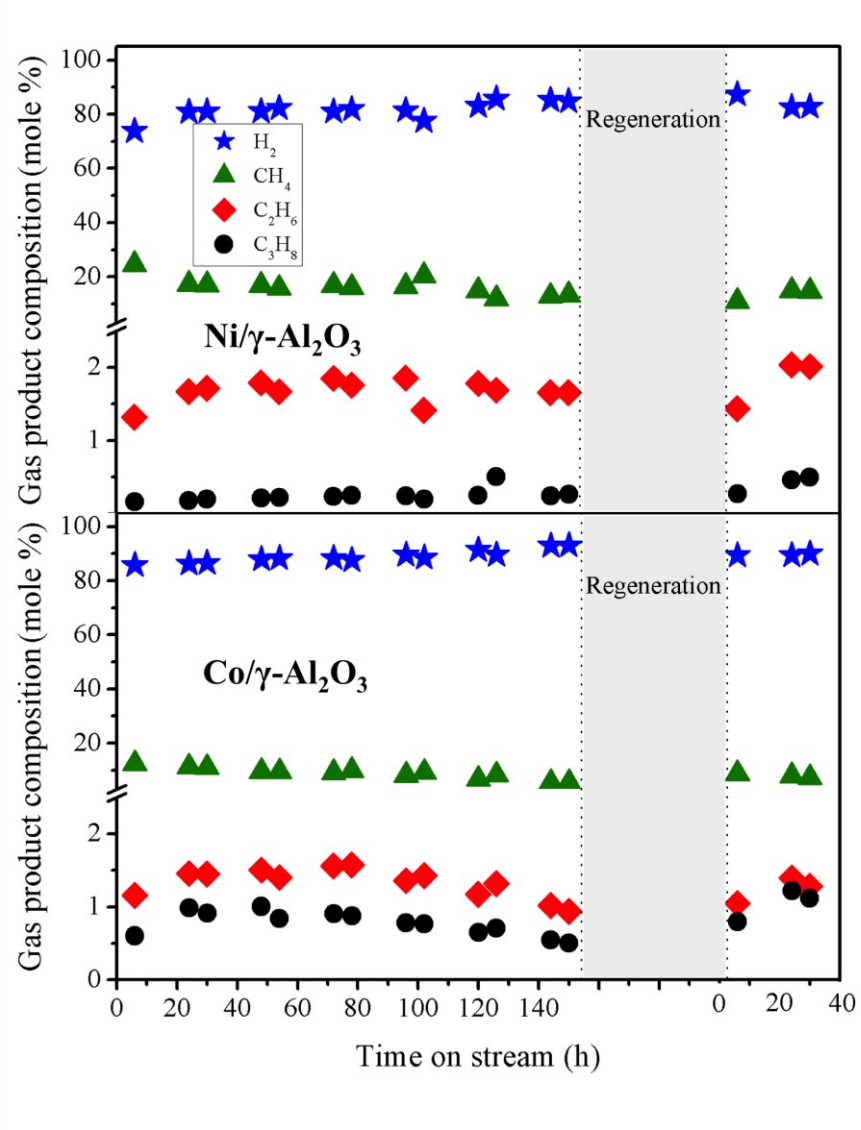

Fig. 4. Gas product composition over time on stream during palm oil hydrodeoxygenation on the catalytic performance and regeneration of the Ni/γ-Al_2O_3 and Co/γ-Al_2O_3 catalysts. Reaction conditions: 573 K, 5 MPa, LHSV of 1 h^{-1}, and H_2/oil ratio of 1,000 N(cm^3/cm^3)

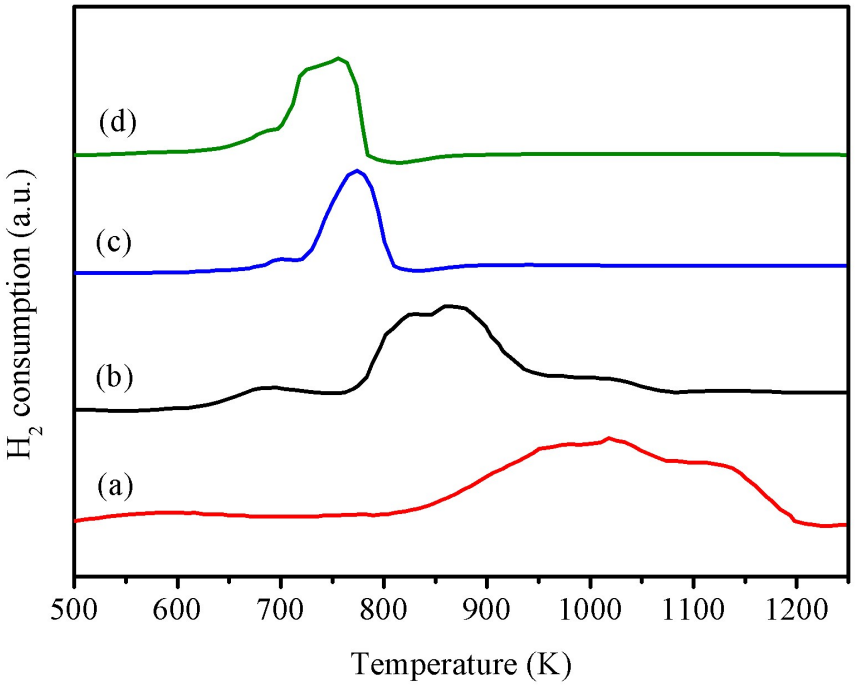

Fig. 5. H_2-TPR profiles of the catalysts, (a) Ni/γ-Al_2O_3, (b) Co/γ-Al_2O_3, (c) NiO, (d) Co_3O_4

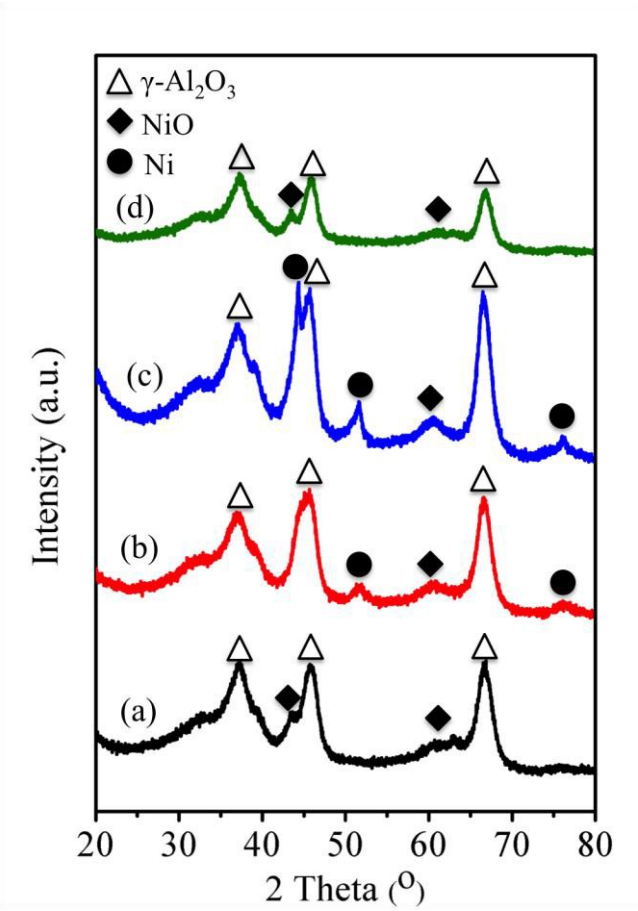

Fig. 6. XRD patterns of the (a) calcined, (b) prereduced, (c) spent, and (d) regenerated of Ni/γ-Al_2O_3 catalysts.

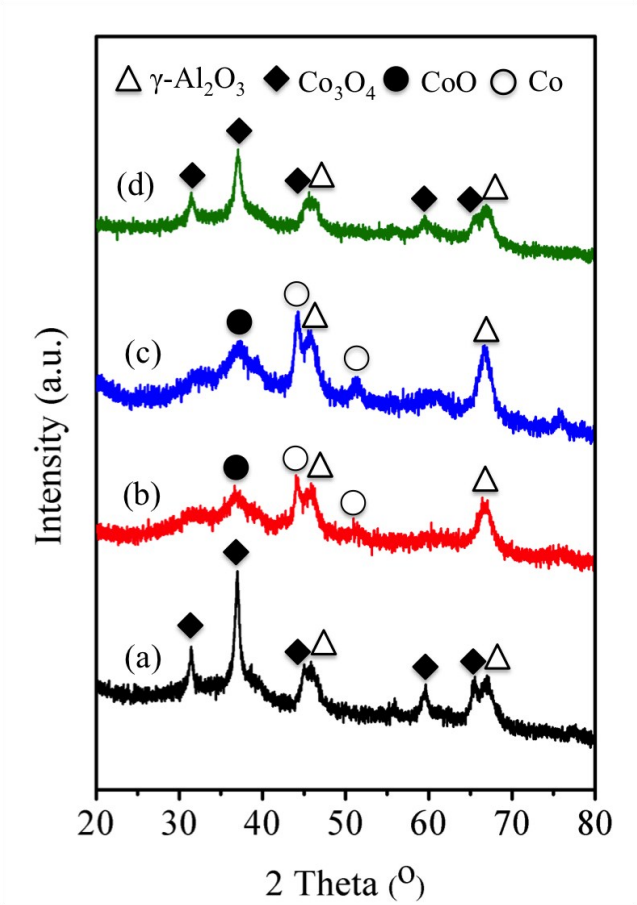

Fig. 7. XRD patterns of the (a) calcined, (b) prereduced, (c) spent, and (d) regenerated of $Co/\gamma\text{-}Al_2O_3$ catalysts.

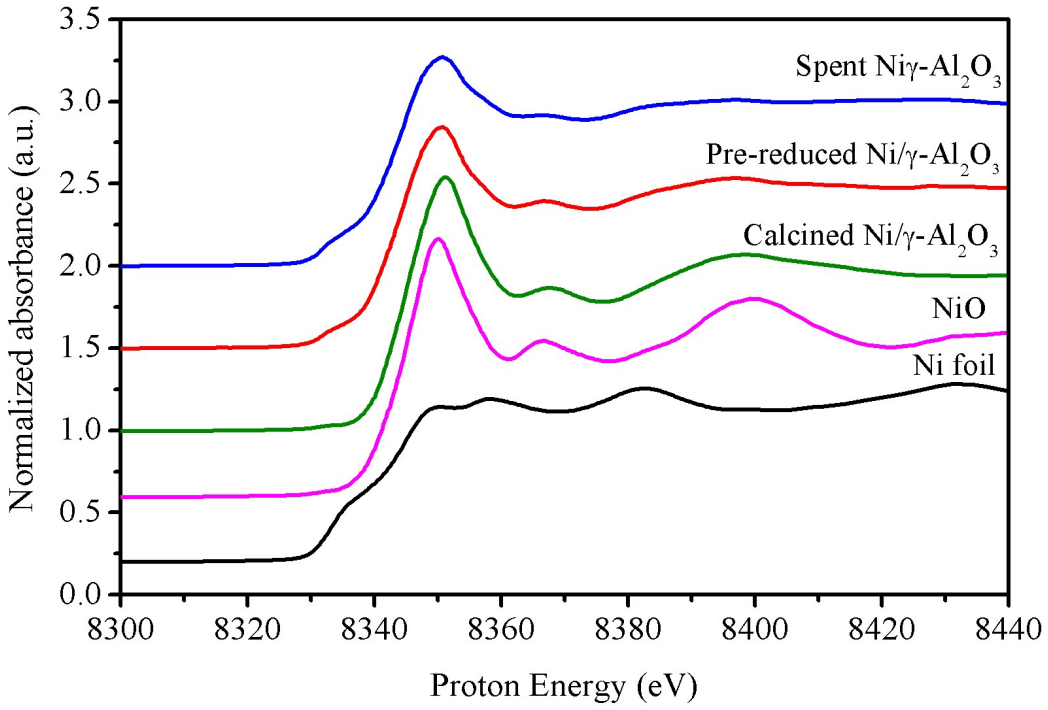

Fig. 8. Normalized Ni K-edge XANES spectra of the calcined, prereduced, and spent Ni catalysts and the reference standards.

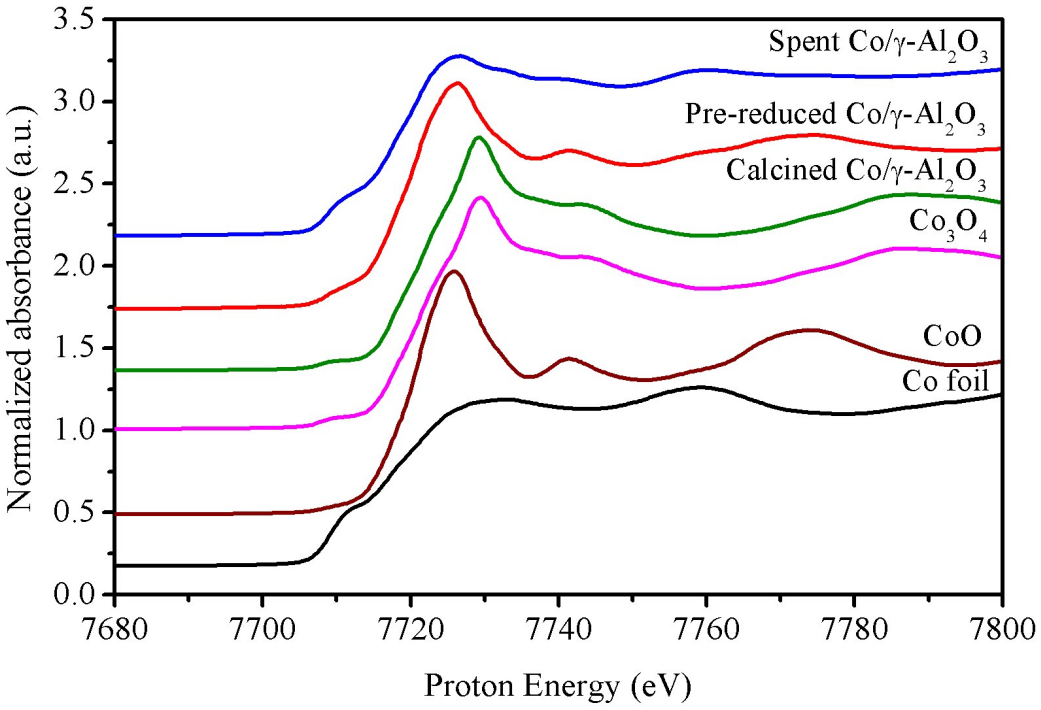

Fig. 9. Normalized Co K-edge XANES spectra of the calcined, prereduced, and spent Co catalysts and the reference standards.

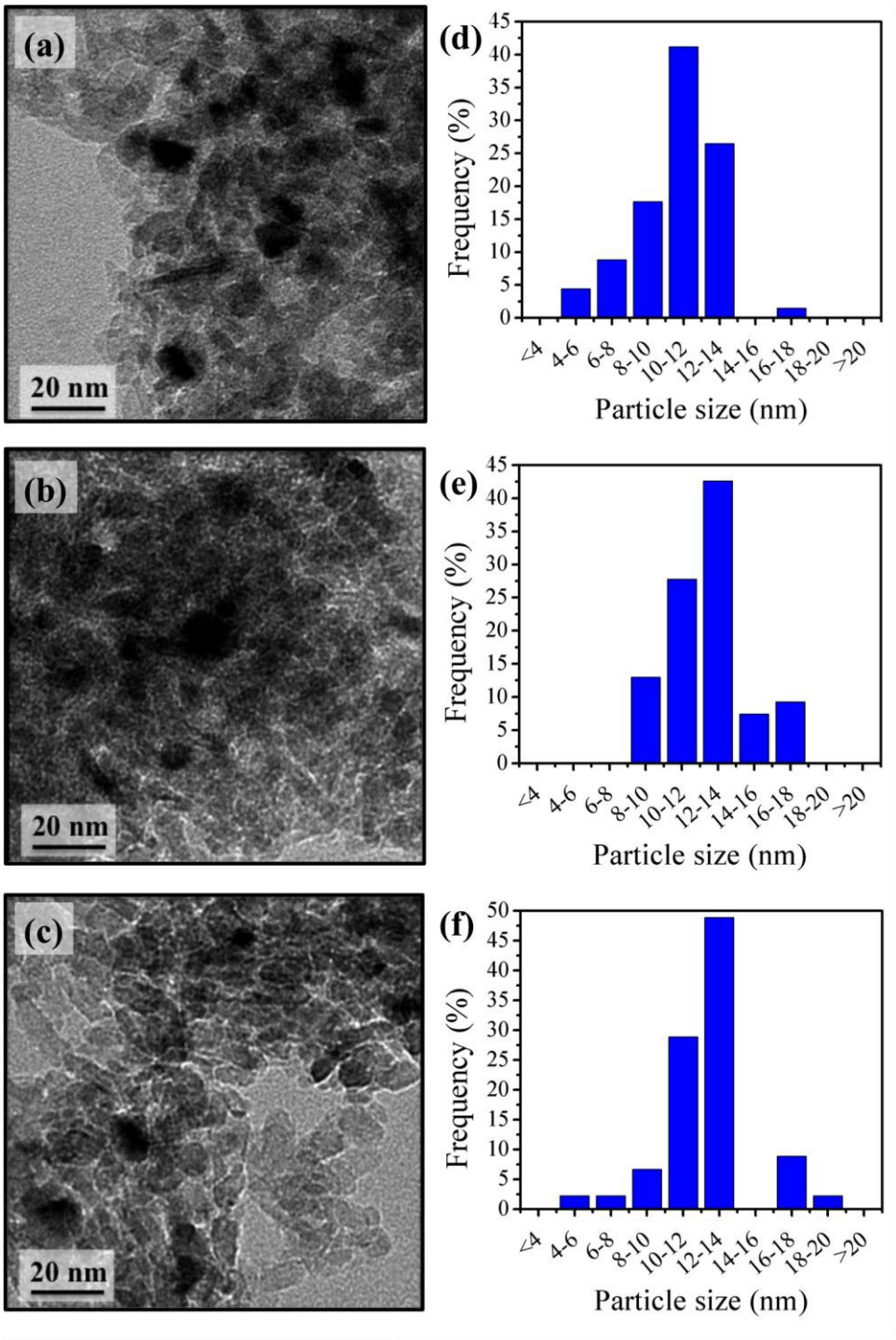

Fig. 10. TEM images of the (a) prereduced, (b) spent, and (c) regenerated Ni/γ-Al_2O_3 and the particle size distribution of the (d) prereduced, (e) spent, and (f) regenerated Ni/γ-Al_2O_3.

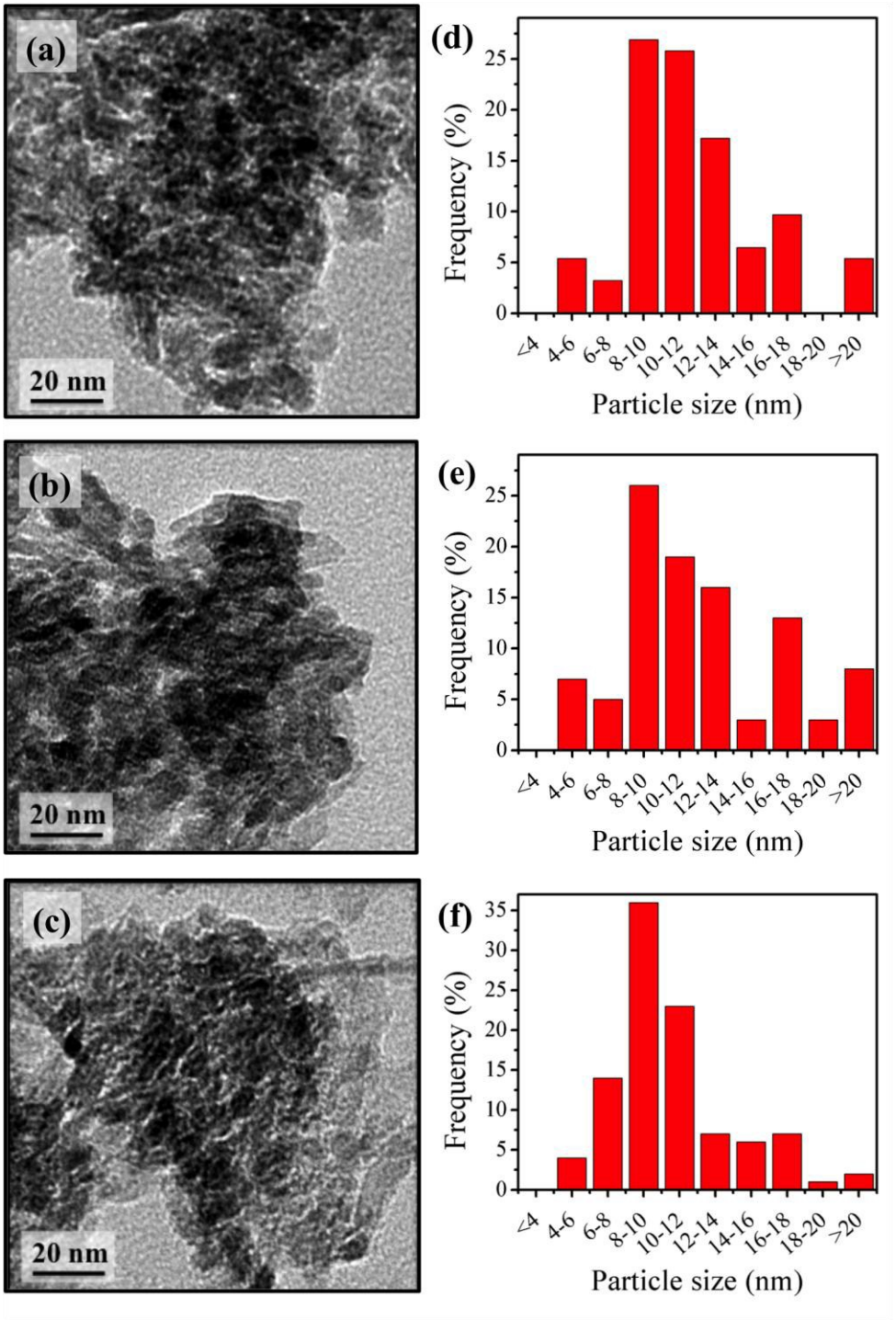

Fig. 11. TEM images of the (a) prereduced, (b) spent, and (c) regenerated Co/γ-Al_2O_3 and the particle size distribution of the (d) prereduced, (e) spent, and (f) regenerated Co/γ-Al_2O_3.

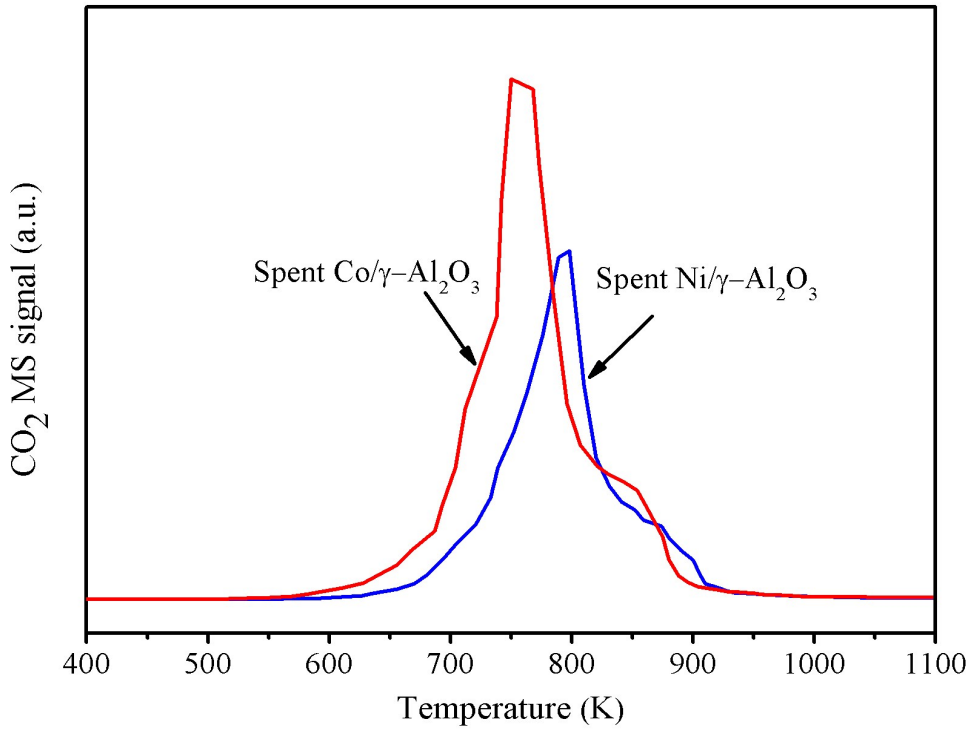

Fig. 12. Temperature programmed oxidation profiles of the Ni/γ-Al_2O_3 and Co/γ-Al_2O_3 catalysts after 150 h on-stream.